Ice-induced vibrations of the Norströmsgrund lighthouse

Torodd Nord[1,2], Ilija Samardzija[1], Hayo Hendrikse[3], Morten Bjerkås[1], Knut V. Høyland[1], Hongtao Li[1]

[1] Sustainable Arctic Marine and Coastal Technology (SAMCoT), Centre for Research-based Innovation (CRI), Norwegian University of Science and Technology, Trondheim, Norway

[2] The University Centre in Svalbard (UNIS), Longyearbyen, Spitsbergen

[3] Delft University of Technology, Delft, The Netherlands

Abstract

The signature and occurrence of frequency lock-in (FLI) vibrations of full-scale offshore structures are not well understood. Although several structures have experienced FLI, limited amounts of time histories of the responses alongside measured met-ocean data are available in the literature. This paper presents an analysis of 61 measured events of resonant vibrations of the Norströmsgrund lighthouse from 2001 until 2003. The vibrations of most of these events did not reach a steady state; thus, they violate an often-quoted criterion for frequency lock-in vibrations and remain outside any modes of ice-induced vibrations suggested in standards.

Met-ocean data from both in situ measurements and from the Copernicus marine service information database are further used to better understand the occurrence of resonant ice-induced vibrations. All events between 2001 and 2003 occurred during days with ice concentrations of 8-10/10, closely packed consolidated drift ice. The locally measured ice velocity and thickness ranged from 0.023 to 0.075 m s^{-1} and from 0.26 to 1.9 m, respectively. These measurements included level ice, rafted ice and ridged ice. The events of resonant vibrations are further compared with measurements from the same structure between 1979 and 1988. Most events of resonant vibrations were recorded in the winter of 1988, followed by the

[1] Corresponding author
E-mail address: torodd.nord@ntnu.no (Torodd S. Nord)

winters of 2003 and 1980. The winter of 1988 had fewer freezing degree days (FDD) than did the 65-year average, whereas the winters of 2003 and 1980 had more FDD than did the 65-year average.

Keywords:

Ice-induced vibrations

Resonant vibrations

Frequency lock-in

Norströmsgrund lighthouse

1 Introduction

Structures exposed to drifting ice may experience ice-induced vibrations (IIV). These vibrations may cause fatigue damage of offshore structures and discomfort for personnel. IIV are a result of the dynamic interaction between ice and structure, mostly associated with crushing failure at the ice-structure interface. The three regimes of IIV are defined as intermittent crushing, frequency lock-in (FLI) and continuous brittle crushing (ISO, 2010). These regimes are typically observed for different ice speeds for a structure interacting with level ice, where intermittent crushing occurs for low ice speeds, FLI occurs for intermediate ice speeds, and continuous brittle crushing occurs for high ice speeds (Yue et al., 2009). FLI is the most violent regime, characterized by Hendrikse (2017) as periodic oscillations near one of the natural frequencies of the structure, while the ISO/FDIS 19906 standard states that FLI causes typically sinusoidal responses at the top of the structure when the ice failure frequency is locked at one of the lowest modes of the structure (ISO, 2010). The FLI term is, however, not unique to describe this phenomenon; this non-uniqueness originates from the physical interpretation in terms of mechanical oscillations. Peyton (1967) and Blenkarn (1970) measured IIV on structures in the Cook-Inlet, from which Blenkarn introduced terminology such as steady-state oscillations and resonant self-excited vibrations to the ice-structure interaction community. These terms are used as alternative definitions for what we usually refer to as FLI (ISO, 2010), and they are often presented alongside with phenomenological models to predict IIV, see Sodhi (1988) and Hendrikse and Metrikine (2015) for an overview. Määttänen (1975) measured FLI on the KEMI-1 steel lighthouse in both the first and second modes of the structure. Only months after deployment in the Gulf of Bothnia, the structure collapsed because of IIV. FLI has been measured on narrow structures (Määttänen, 2008; Nordlund et al., 1988), wide structures (Jefferies and Wright, 1988) and jacket structures (Yue and Bi, 2000). Despite the structural differences, the response signals share the rise of high-amplitude oscillations near a natural frequency. Examples of this phenomenon can be seen when comparing selected responses from the Norströmsgrund lighthouse (Nord et al., 2016) and from the MS jacket platform (Yue and Bi, 2000). Because of the limited selection of signals in publications, these are often cases for which there is practically no doubt whether they belong to FLI and result in little discussion on the actual classification. Cases of vibrations near a natural frequency of a structure that violate the steady-state oscillations also violate the ISO 19906 (ISO, 2010) definition of FLI, which states that the response inherits a sinusoidal shape.

In this paper, resonant vibrations are used as a common term for vibrations near a natural frequency of the structure, which also includes FLI, and hence, no specific type of oscillator is assigned to the ice-structure interaction system (Rajasekar and Sanjuan, 2016). We show the encountered difficulty to classify IIV events as FLI when we present an analysis of 61 events of resonant vibrations that were measured on Norströmsgrund lighthouse between 2001 and 2003.

The signatures in the measured structural responses are discussed alongside the ice conditions under the occurrences of these events and the inherent uncertainties in the measurements and analysis. The 61 events are compared to earlier measurements of resonant vibrations on the same structure (Engelbrektson, 1987a; Engelbrektson, 1987b; Engelbrektson, 1989; Engelbrektson and Janson, 1985), which together total more than 200 events.

2 Measurements

This chapter briefly describes two measurement campaigns on the Norströmsgrund lighthouse: one in the time period 2001-2003 and another in the time period 1979-1988. The differences in measurement techniques between the two measurement campaigns affect the current results to an unknown extent and are almost impossible to quantify because the measurement techniques varied from year to year, and often uncertainties in the measurements vary between the different ice conditions. Table 1 summarizes how structural response, ice thicknesses and ice velocities were measured.

2.1 Instrumentation, measurements and post-processing of data on Norströmsgrund 2001-2003

The STRICE (STRuctures In ICE) measurements in 2001-2003 were published in reports (e.g., Haas et al., 2003; Kärnä and Yan, 2009), a thesis (Bjerkås, 2006a) and several papers that discuss more detailed events of IIV (e.g., Bjerkås, 2006b; Bjerkås et al., 2013b), events of ice ridge actions (Bjerkås and Bonnemaire, 2004), failure modes (Kärnä and Jochmann, 2003) and mechanical properties (Fransson and Stenman, 2004). Fig. 1 displays the accelerometer locations on the lighthouse and a picture of Norströmsgrund surrounded by ice. Measurements were also performed in 1999 and 2000; however, these measurements are herein excluded because they lack acceleration measurements. Because instrumentations changed from year to year, figures of all instrumentation configurations are not provided here; see Bjerkås (2006a) for details.

All events that were judged resonant types of vibrations are given in Table 2, wherein necessary information is provided for the reader to examine the instances in the original data set.

The ice thickness at lighthouse Norströmsgrund was measured both with an upward-looking sonar (ULS) and an electromagnetic (EM) sensor (Haas and Jochmann, 2003). The ULS was mounted 5 m southeast of the lighthouse on the submerged caisson (+7.5 m elevation), and the EM sensor was hung 10 m east of the lighthouse, approximately 2 m above the mean water level (MWL). The ULS recorded the deepest point of the ice, and the ice surface elevation was measured with a laser. The ULS was operational in the winters of 2000 and 2001. The EM thickness was estimated based on a 6-m diameter measurement footprint, and the estimates depended on the ice conductivity. More information regarding these measurements can be found in Haas (2000).

Although the ice thickness was measured at a certain time, it could take minutes before that ice appeared at the ice-structure interface. The heterogeneity of the ice cover was also a complicating factor in the ice-thickness estimation because the ice underneath the EM sensor, or above the ULS, was at times different than the ice at the ice structure interface. Video records were then used to estimate the ice thickness at the ice-structure interface.

Ice thickness measurements, video records and freezing degree days (FDDs) were used to judge the types of ice features (level, rafted, or ridged ice) that interacted with the lighthouse during an event of resonant vibrations. The number of FDDs was calculated based on air temperature measurements at both Luleå Airport and the Rödkallen meteorological station. The daily mean temperatures were calculated using the Ekholm-Modèn model that uses weighted averages of the minimum and maximum temperatures as well as the temperatures measured at 7 am, 1 pm and 7 pm. See Li et al. (2016) for more details.

EU Copernicus Marine Service Information was used to estimate the local ice concentrations and ice thicknesses. This information database provided reanalysis using the HIROMB (High-Resolution Operational Model of the Baltic) model, which may be used to provide mean values for every 6 hours of a variety of met-ocean data. HIROMB has a spatial resolution is 5.5 km, and the model error (mean RMSE) is 0.08 m and 0.2 for level ice thickness and ice concentration, respectively (Axell et al., 2017). Note that the model takes into account deformed ice; however, the error is unknown.

Video footage was used in conjunction with an ice drift tracking routine (Leese et al., 1971; Samardzija, 2018) to obtain the ice velocities during the events of resonant vibrations. This process was necessary because logbook values of ice velocities were often not written at the time during events, and video records clearly showed changes in ice velocity. Instances when ice velocities were written into the data logbook were used as benchmark values for the image correlation routine. The routine compares two subsequent grayscale frames by taking a subsection of one image and moving it stepwise on top of the other image until a perfect overlap is found. A bivariate correlation coefficient is calculated between the image subsection and the underlying image for each step and further populated into a two dimensional matrix. Each matrix element corresponds to a specific spatial lag in horizontal and vertical direction. The matrix element with the maximum correlation coefficient is proportional to the displacement vector of the ice surface, from which we obtained the ice velocity.

Accelerometers installed at +16.5 m and +37.1 m elevation were used to measure accelerations in two directions in the horizontal plane. The sampling frequency varied from 1 to 100 Hz. Some events with low sampling frequency that showed tendencies to resonant vibrations were excluded from further analysis because the low sampling frequency made it too difficult to interpret the signals. Whenever filters or resampling routines are applied in this paper, it is specified in the text. Nine panels measured local ice forces and covered the outer perimeter from 0 to 162°. Global ice forces can be estimated from the panels (Nord et al., 2016); however, such estimation is outside the scope of this paper.

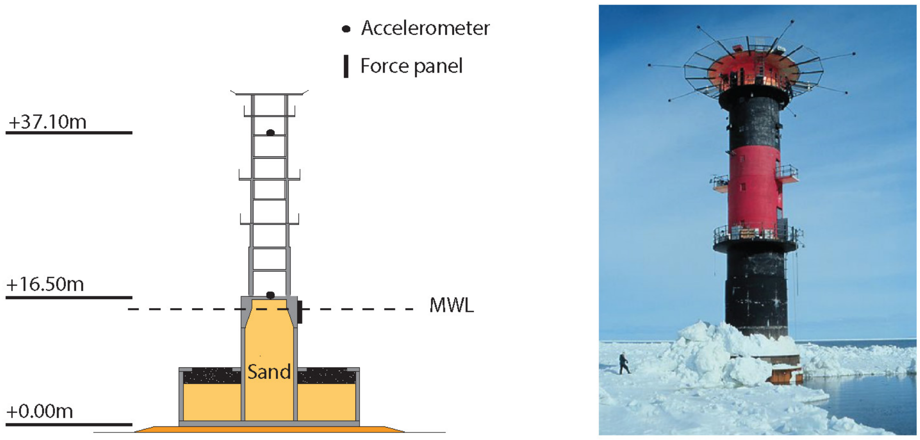

Fig. 1. Illustration of the accelerometer and force panel locations and picture of the Norströmsgrund lighthouse.

2.2 Supplementary measurements from reports: Norströmsgrund 1979-1988

The Norströmsgrund lighthouse was equipped with accelerometers on two levels to measure the structural vibrations since the winter of 1973, after service staff noticed that the structure oscillated. The first records of resonant vibrations were published in Engelbrektson (1977), in which he reported the maximum recorded accelerations on the lighthouse to be 0.33 g. Every time the accelerations exceeded 0.07 g, the system stored time histories automatically. In 1980, video footage was included in the measurements, but the acceleration trigger level was kept to 0.07 g. A summary of the measurement program is given in the publication of Engelbrektson (1983), which includes a description of the strongest event of resonant vibrations ever recorded on the Norströmsgrund lighthouse that occurred on February 28, 1979 at 14.54 h. The same event was also described in a later publication (Engelbrektson and Janson, 1985).

Table 1. Measurement methods.

Measurement type	Accelerations	Ice thickness	Ice velocity

Method 1979-1988	Automatically activated at 0.07 g (1979-1985) and 0.03 g (1985-1988) (Engelbrektson, 1983; Engelbrektson, 1987b; Engelbrektson and Janson, 1985).	Reported from ice breakers and available ice charts (Engelbrektson, 1987a).	Measurements from ice breakers and calculations based on forecast models (Engelbrektson, 1987a).
Method 2001-2003	Manually activated during ice-structure interaction (Bjerkås, 2006a).	Measured by sonar, electromagnetic instruments and laser (Haas et al., 2003).	Measured using grid on the video screens (Jochmann and Schwarz, 1999).

3 Methods

3.1 The signature 2001-2003

This section aims to show how the time series of acceleration measurements were used to define an event of resonant vibrations. The inherent features in the signals are called the *signature.* The criteria for considering a time series as a resonant vibration event were that the response showed a) an increase of the amplitude, and b) the dominant response was close to a natural frequency of the structure. Because the natural frequencies are in fact unknown and may be closely separated (Nord et al., 2017; Nord et al., 2016), we assumed that responses with a dominant frequency between 2.0-2.7 Hz could be considered as resonant vibrations. The events were first selected by visual inspection of all the acceleration response time series in the STRICE data set. When high amplitudes were observed, the response dominant frequency component was verified by examining the first singular value of the cross power spectral densities (Fig. 2): the cross power-spectral densities were calculated from the four acceleration time histories. Thereafter, the singular values were extracted using a singular value decomposition (SVD) and plotted against frequency.

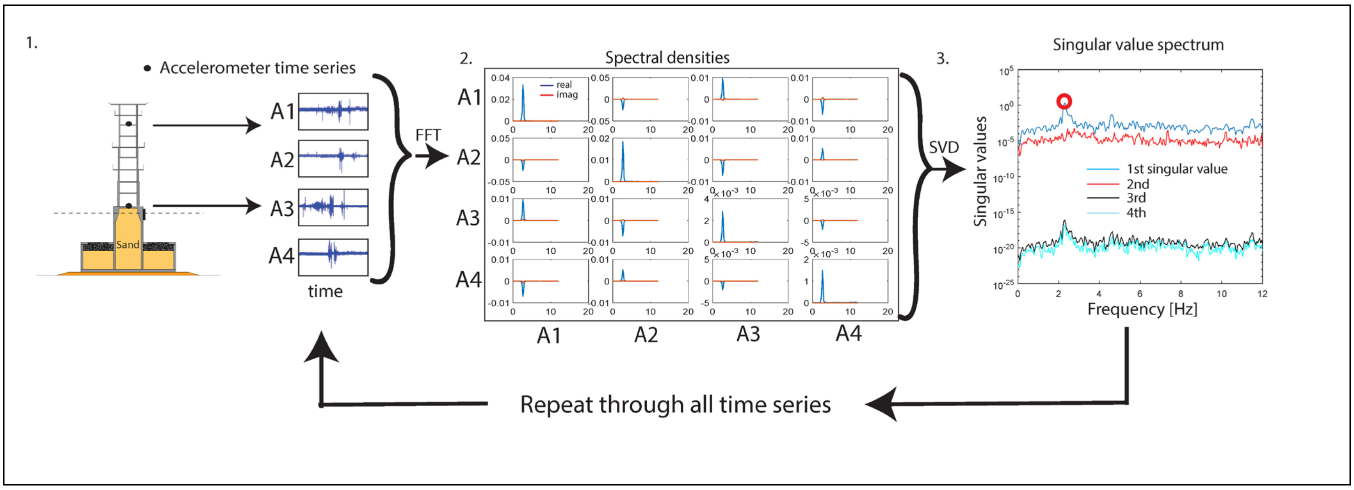

Fig. 2. Schematic of the data processing flow.

The majority of events had variable amplitudes, making it difficult to well-define the durations of the individual events: One example that illustrates the variability of the response amplitudes and thus the difficulty to choose an event length is shown in Fig. 3. Here, the response fulfilled the requirement of a dominant frequency component; however, the response amplitudes are small, when compared in particular to the highest acceleration ever recorded of 6 m s^{-2}. When all events were resampled down to 10 Hz, the power spectral densities showed that most events had dominant frequencies between 2.2-2.4 Hz. Three events showed a dominant frequency at 2.7 Hz, and one event showed a dominant frequency at 2 Hz.

For years 1979-1988, no digital data was available, and the judgment is based on statements of *"resonant vibrations"* and inspection of the plotted time histories of acceleration in the appendices of Engelbrektson (1987a) and Engelbrektson (1989). Note that, in what follows, the numbers of days and events of resonant vibrations are uncertain and depend on both the measurement system and the level of details in the reports.

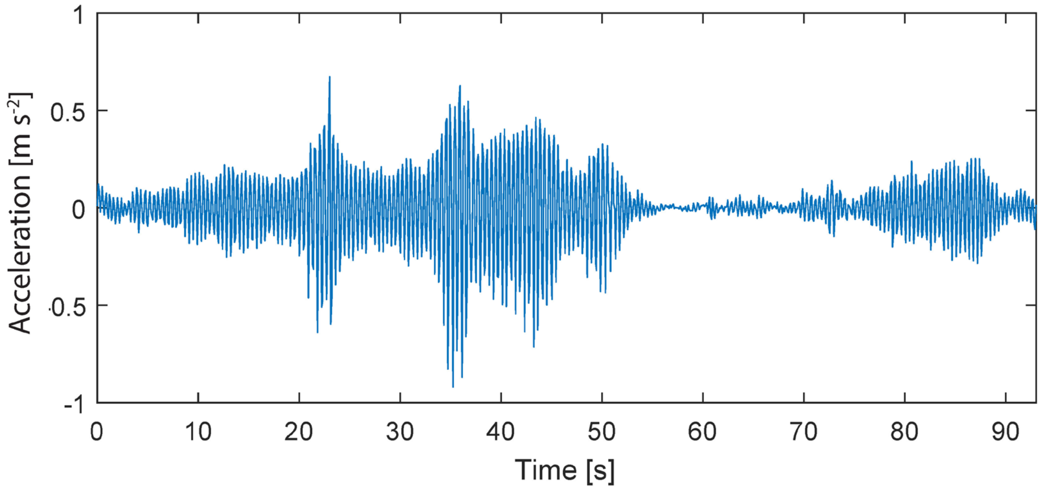

Fig. 3. Response during a low-amplitude resonant vibration event (# 44 in Table 2).

4 Results

4.1 Seasonal overview from 1979-2003

The 37 days in which resonant vibrations were measured (and reported) are plotted against FDD in Fig. 4 a. The cold winters, 1979, 1980 and 1981 all had two days when resonant vibrations were measured. Based upon the available literature, no projects were assigned to the winter of 1982; this lack of projects may also explain why no events were reported. The warmest winter (1983) had two days when resonant vibrations were measured. During the winters of 1984 and 1985, no accelerations exceeded 0.07 g (Engelbrektson, 1987a). In the winters of 1986 and 1987, no resonant vibration events of interest were recorded (Engelbrektson, 1989). The winter of 1988, which was slightly warmer than the 65 year average (Li et al., 2016), had 13 such days of resonant vibrations and the largest number of events, followed by the winters of 2003 and

1980 (Fig. 4b). The earliest events occurred in January, and the latest occurred in May; most events occurred during March, followed by February and April (Fig. 4b).

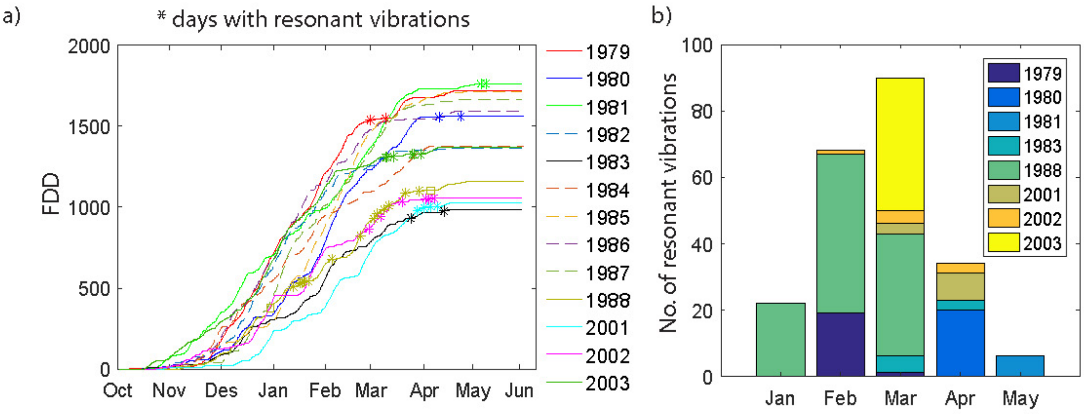

Fig. 4. Seasonal overview of resonant vibration events: a) freezing degree days and days with resonant vibrations from 1979-2003 according to Li et al. (2016); b) number of events per month for different years.

4.2 Results from measurements 2001-2003

In total, 61 events of resonant vibrations were identified in the data from 2001-2003 (Table 2). Figures of the upper level acceleration (cf. Fig. 1) for all events are given in Appendix 1. Except for the dominant frequency component, the response and force time histories varied notably. A steady-state response with constant amplitudes seldom occurred. At times, the response appeared close to steady-state; however, with closer inspection, the amplitudes changed from cycle to cycle.

Table 2. Events of resonant vibration measured between 2001 and 2003.

No.	Date of event [DD.MM.YYYY]	Data file id	Start time [hhmmss]	End time [hhmmss]	Ice thickness [m]	Ice velocity [m s^{-1}]	Peak acceleration [m s^{-2}]	10 peaks average accelaration [m s^{-2}]
1	28.03.2001	01_2803_0300	081123	081132	0,33	0,028	0,31	0,27

2	28.03.2001	01_2803_0300	084230	084237	0,26	0,028	0,70	0,34
3	28.03.2001	01_2803_0300	090538	090547	0,27	0,028	0,60	0,41
4	01.04.2001	01_0104_0400	093357	093405	0,40	0,046	1,40	1,07
5	01.04.2001	01_0104_0400	093847	093927	0,40	0,038	1,63	1,24
6	05.04.2001	01_0504_0400	154755	154802	0,90	0,075	1,65	1,31
7	09.04.2001	01_0904_0400	223741	223807	0,63	0,050	1,69	1,43
8	09.04.2001	01_0904_0400	223830	223845	0,66	0,050	1,03	0,78
9	09.04.2001	01_0904_0400	223920	223953	0,57	0,050	2,13	1,84
10	09.04.2001	01_0904_0400	224012	224023	0,62	0,050	0,96	0,76
11	09.04.2001	01_0904_0400	224157	224233	0,65	0,050	1,66	1,52
12	27.02.2002	02_2702_0200	191534	191612	1,67	0,041	0,31	0,27
13	06.03.2002	02_0603_0100	002310	002345	0,78	0,051	2,15	1,37
14	19.03.2002	02_1903_0700	215818	215830	0,60	0,026	0,67	0,52
15	19.03.2002	02_1903_0700	220044	220102	0,60	0,023	1,00	0,87
16	19.03.2002	02_1903_0700	220600	220610	0,60	0,024	0,45	0,37

17	02.04.2002	02_0204_0200	064842	064856	0,40	0,026	1,11	0,67
18	04.04.2002	02_0404_0200	103826	103847	0,40	0,027	1,08	0,60
19	04.04.2002	02_0404_0300	104315	104323	0,48	0,027	0,82	0,58
20	07.04.2002	02_0704_0200	54040	054046	1,08	0,042	0,81	0,50
21	09.03.2003	03_0903_0200	005607	005640	0,60	0,041	1,57	1,18
22	09.03.2003	03_0903_0200	010023	010040	0,60	0,059	1,98	1,46
23	09.03.2003	03_0903_0200	010340	010401	0,60	0,048	1,41	1,20
24	10.03.2003	03_1003_0200	035915	035922	0,73	0,056	2,54	1,24
25	10.03.2003	03_1003_0200	040112	040118	0,79	0,058	0,90	0,58
26	10.03.2003	03_1003_0200	040136	040142	0,79	0,058	0,55	0,40
27	14.03.2003	03_1403_0400	221620	221627	0,80	0,037	0,36	0,32
28	25.03.2003	03_2503_0600	153247	153258	0,90	0,052	1,92	1,18
29	25.03.2003	03_2503_0600	153343	153403	0,98	0,050	2,24	1,57
30	25.03.2003	03_2503_0600	153617	153623	0,95	0,052	1,44	1,05
31	25.03.2003	03_2503_0600	153640	153653	0,95	0,051	1,73	1,34

32	25.03.2003	03_2503_0600	153708	153722	0,93	0,053	1,60	1,28
33	25.03.2003	03_2503_0600	154318	154327	0,89	0,054	0,82	0,73
34	25.03.2003	03_2503_0600	155658	155743	0,88	0,045	1,58	1,29
35	25.03.2003	03_2503_0600	160101	160105	0,86	0,043	1,60	0,95
36	25.03.2003	03_2503_0600	160234	160240	0,95	0,039	0,75	0,63
37	25.03.2003	03_2503_0600	160632	160751	1,08	0,041	1,77	1,58
38	25.03.2003	03_2503_0600	162054	162139	0,98	0,042	1,15	1,11
39	25.03.2003	03_2503_0600	162255	162305	0,98	0,041	0,93	0,78
40	25.03.2003	03_2503_0600	163159	163212	0,86	0,040	1,02	0,92
41	25.03.2003	03_2503_0600	170523	170530	0,84	0,031	0,90	0,67
42	25.03.2003	03_2503_0600	171120	171130	0,88	0,027	1,16	0,91
43	25.03.2003	03_2503_0600	171242	171253	0,84	0,027	0,85	0,62
44	25.03.2003	03_2503_0700	192148	192320	1,50	0,036	1,00	0,79
45	25.03.2003	03_2503_0700	192448	192514	1,90	0,035	0,54	0,47
46	26.03.2003	03_2603_0200	121746	121825	1,00	0,043	0,73	0,58

47	26.03.2003	03_2603_02 00	122829	122955	1,00	0,040	0,99	0,85
48	26.03.2003	03_2603_02 00	123118	123218	1,00	0,031	0,92	0,78
49	30.03.2003	03_3003_04 00	120338	120352	0,91	0,037	0,76	0,54
50	30.03.2003	03_3003_04 00	120524	120539	1,03	0,038	1,13	0,90
51	30.03.2003	03_3003_04 00	120547	120624	0,90	0,041	1,52	1,18
52	30.03.2003	03_3003_04 00	121419	121431	0,88	0,047	1,09	0,87
53	30.03.2003	03_3003_04 00	121500	121514	0,91	0,047	1,26	0,99
54	30.03.2003	03_3003_04 00	121738	121748	0,87	0,045	0,65	0,58
55	30.03.2003	03_3003_04 00	122538	122700	0,70	0,049	1,96	1,82
56	30.03.2003	03_3003_04 00	122950	123007	0,80	0,050	0,99	0,82
57	30.03.2003	03_3003_04 00	123301	123311	0,70	0,052	0,86	0,58
58	30.03.2003	03_3003_04 00	124243	124253	0,77	0,051	0,58	0,41
59	30.03.2003	03_3003_05 00	125818	125847	0,78	0,053	0,73	0,61
60	30.03.2003	03_3003_05 00	130144	130148	1,20	0,053	0,85	0,61
61	30.03.2003	03_3003_05 00	130918	130928	1,20	0,057	0,89	0,64

4.2.1 Ice velocity

Several events had significant changes in ice velocity prior to, during and after an event of resonant vibrations, as illustrated in Fig. 5, wherein the acceleration ice velocity and ice thickness are given for April 5, 2001. Here, the event started at 15.47.55 and lasted for approximately 7 seconds, during which the structural responses significantly increased (Fig. 5a), the mean ice velocity was approximately 0.075 m s^{-1} (Fig. 5b) and the ice thickness was approximately 0.9 m (Fig. 5c). When the ice velocity slowed down to zero, the acceleration decreased and resulted in ductile (creep) interaction.

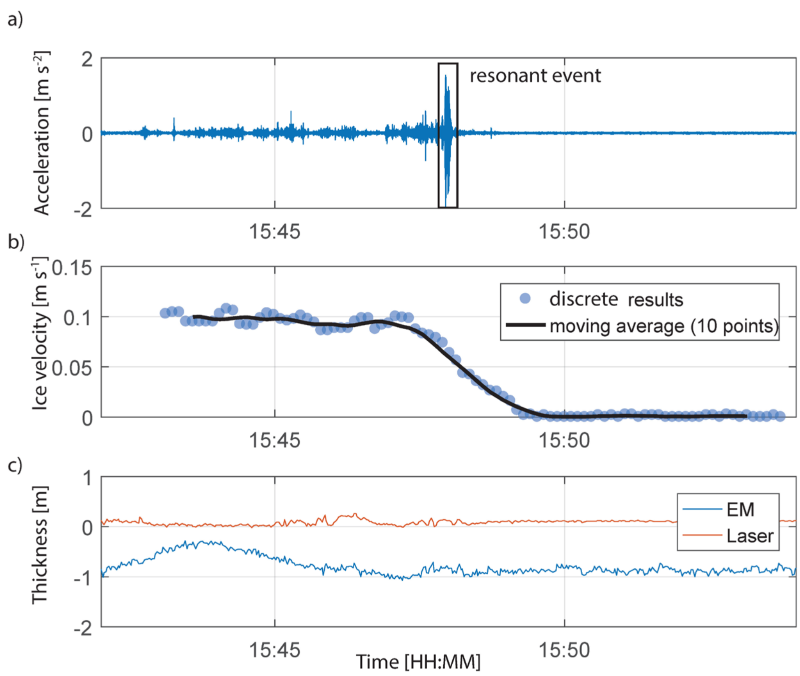

Fig. 5. Acceleration (a), ice-drift velocity (b) and ice thickness (c) on April 5, 2001.

The mean duration of the events was approximately 22 seconds, while only 5 events were longer than 60 seconds (Fig. 6a). The mean ice velocity was 0.043 m s^{-1}; hence, the average event crushed approximately 0.9 m of ice. The highest measured acceleration at the top of the structure occurred with an ice velocity of 0.055 m s^{-1}. The average of the 10 highest acceleration peaks in an event was often significantly lower than the highest peak (Fig. 6b). Note that the accelerations used in this as well as the following figures and text are the absolute values of the two sensors at top and that the acceleration time series are resampled down to 10 Hz to make them comparable with each other. At times, the resampling affected the amplitudes; as a result, quantities derived from the values presented in the figures and Table 2 may be erroneous. The mean of the maximum accelerations at the top for all events was 1.15 m s^{-2}. The events that had ice velocities of less than 0.03 m s^{-1} were primarily caused by ice drift from south and southeast (Fig. 7a), and top accelerations exceeding 2 m s^{-1} occurred with ice-drift from west, southwest, south, southeast and northeast (Fig. 7b). Four out of five events with durations in excess 60 seconds were caused by ice drift from south, while the fifth was caused by ice drift from northeast.

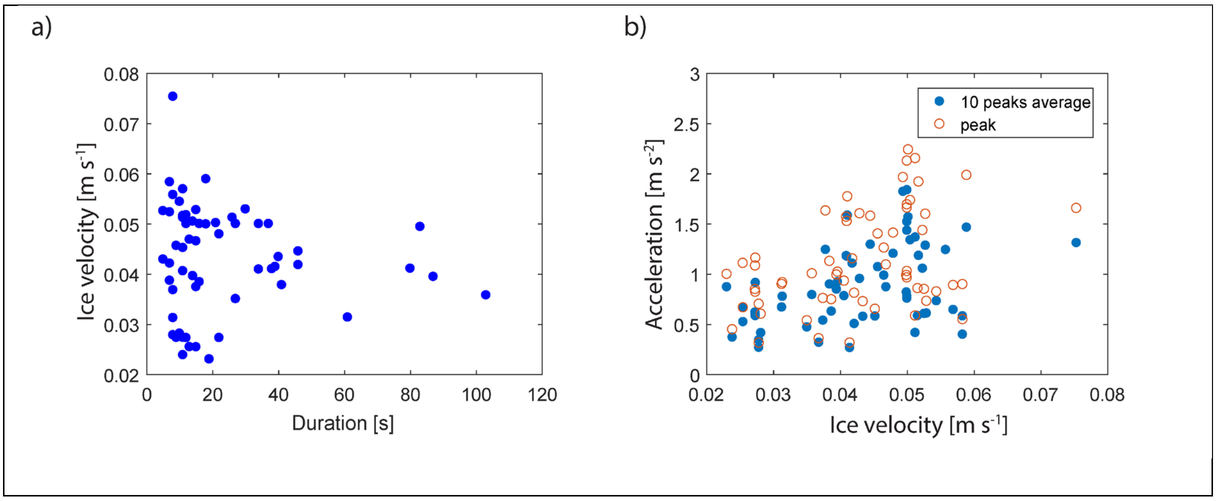

Fig. 6. Ice velocity versus duration of the events (a) and acceleration at the upper level versus ice velocity (b).

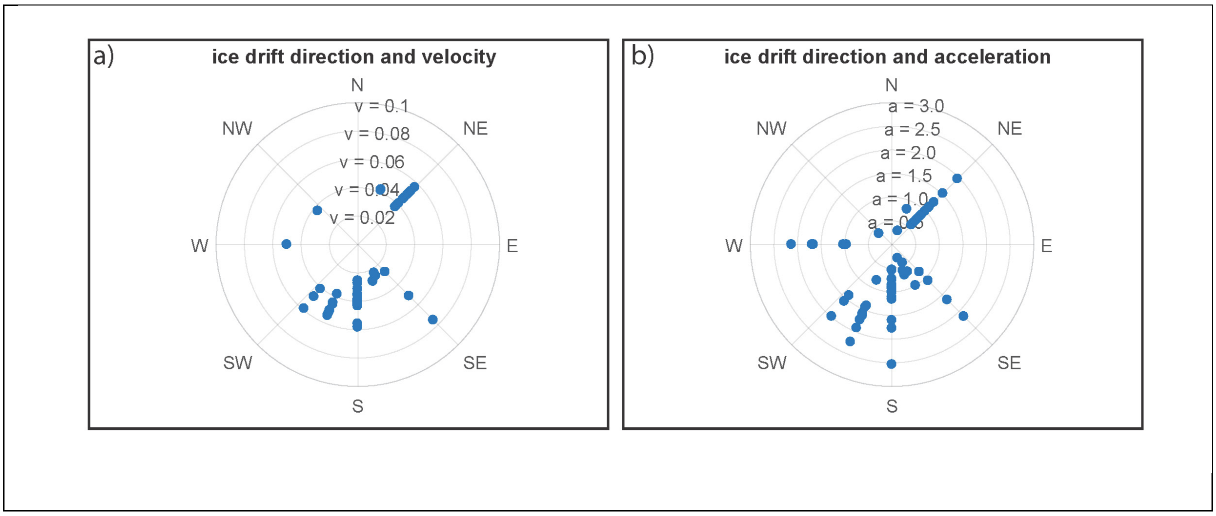

Fig. 7. Ice drift direction versus a) ice velocity and b) event peak acceleration at the top level.

4.2.2 Ice thickness and ice concentration

The six hour mean ice thickness and ice concentration generated using E.U. Copernicus Marine Service Information (E.U.Copernicus, 2017) are given in Fig. 8. The ice thickness measurements in 2001 coincide the most with the model (Fig. 8), whereas measurements in 2002 correspond to the single largest difference between the model and the measurement. All events of resonant vibrations occurred with ice concentrations in excess 0.85. Based on the measured thickness in conjunction with video records, resonant vibrations occurred during interaction with both rafted and ridged ice. Events that lasted longer than a minute occurred for ice thicknesses between 0.7 and 1.5 m (Fig. 9a), and events with the highest accelerations occurred for ice thickness between 0.4 and 1.2 m (Fig. 9b).

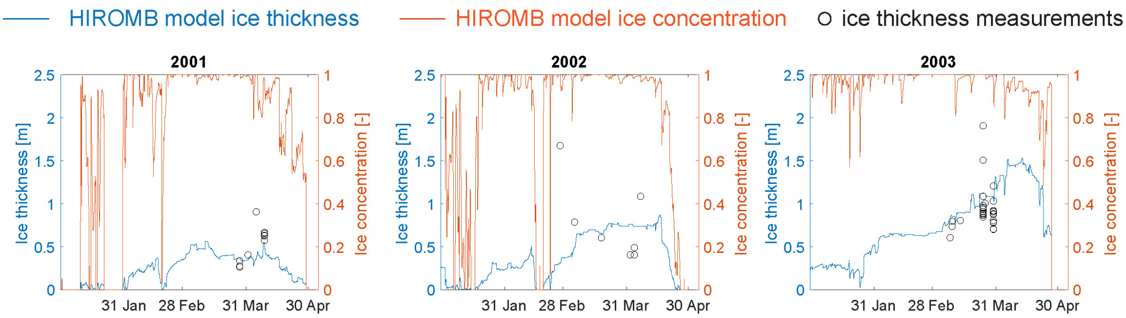

Fig. 8. Ice thickness and ice concentration obtained from the HIROMB model displayed together with ice thickness measurements during the resonant vibrations events.

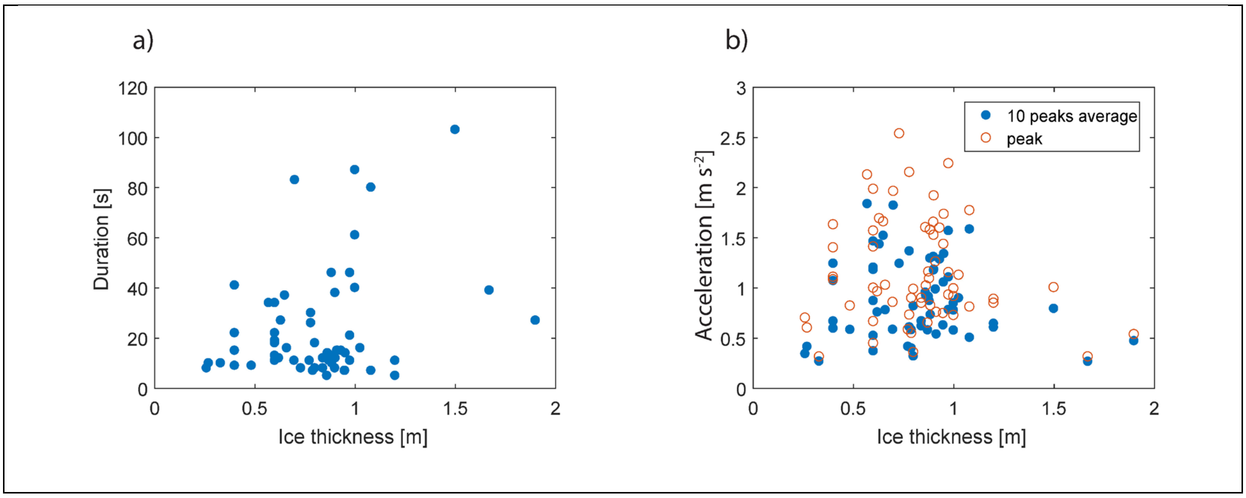

Fig. 9. Event duration versus ice thickness (a) and event peak acceleration at the top level versus ice thickness (b).

5 Discussion

5.1 The signature

For events where the acceleration signal sampling frequency was 30 Hz or higher, it was effective to plot the first singular value of the cross power spectral density of each event in a colormap to determine whether events fulfilled the criterion of a dominant frequency component (Fig. 10a). Each event was also compared with a colormap that was generated using the same method and same sensors but for events in which other failure modes governed the interaction, e.g., flexural failures, splitting, creep, and brittle crushing (Fig. 10b). Nord et al. (2017) explained the details of the selection criteria for these events that were used in a system identification study. The resonant events display a much narrower band between 2.0-2.7 Hz (mostly 2.2-2.4 Hz), whereas other interaction regimes spread the energy over several frequencies.

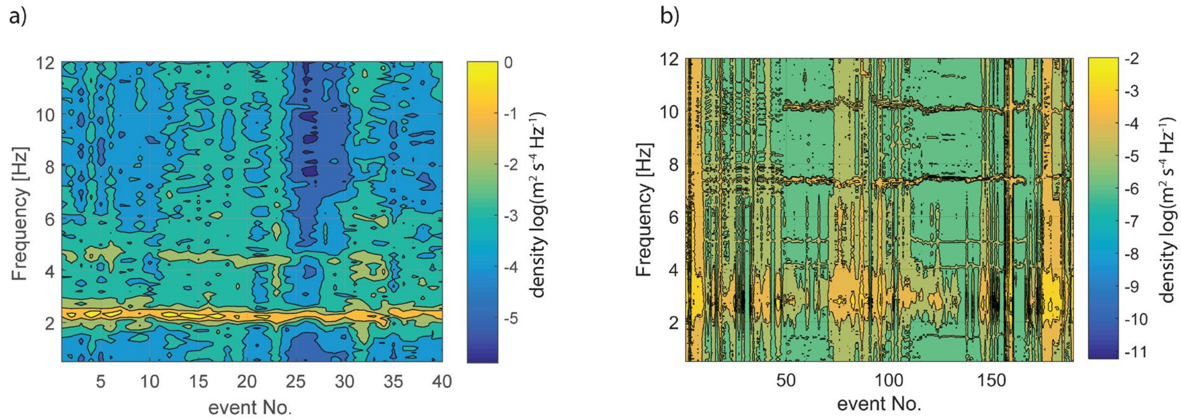

Fig. 10. Singular value colormap of a) resonant vibration events and b) other interaction regimes.

The resonant vibration events had a large range of response amplitudes, partly because of the limited constraints on the selection. At times, the response amplitudes were lower than those for some cases of continuous brittle crushing. Because of the lack of a response amplitude threshold, the duration was dependent on the analyst interpretation. Attempts to better define durations by using response amplitudes from instances in which other failure modes governed the interaction as a lower threshold did not succeed because: a) the response prior to and after an event was often governed by different failure modes (e.g., flexural failure prior to the event and limit-force stalling after the event) and b) the ice conditions were often heterogeneous, resulting in variability in the acceleration response, which made it difficult to decide upon a threshold. Any instance of a sudden global ice failure may also lead to transient responses which may appear as resonant ice-induced vibrations. It is herein assumed that such transient responses would not inherit a response amplitude build up and cycles of sustained high-amplitude vibrations.

Given the wide range of ice velocities and ice thicknesses for which resonant vibration occurred, the observed response differences between resonant vibration events may not be surprising. If the crushing failure process is sensitive to small variations in the ice conditions, so will the response. It was, however, difficult to determine the failure process from the video records. Panel forces may be used as a means to study how the level of synchronization between the panel forces affects the resonant vibration events. Such a study requires careful treatment of the varying sampling frequency between the events and falls outside the scope of this paper. In addition, in many of the 61 events, the ice approached from directions in which the lighthouse had no or limited coverage of load panels.

Määttänen (1975) and Nordlund et al. (1988) also reported differences among FLI type of ice-induced vibration. The latter measured 29 events of FLI on the KR11 channel marker, from which events were subdivided into high and low-level amplitudes. The lower the amplitudes, the more random were the vibrations. The durations varied between 2 and 53 minutes and often occurred with long periods of steady-state response (Kärnä, 1994; Nordlund et al., 1988). For offshore structures in the Bohai Bay, steady-state vibrations are also a common signature of measured FLI events (Yue et al., 2009), with durations up to 10 minutes (Yue et al., 2002). At Norströmsgrund, most events were less than 20 seconds, and few showed steady-state vibrations. Examples of steady-state vibrations can be found in Appendix 1 in Engelbrektson (1987a). The most violent event of resonant vibration measured on Norströmsgrund showed, however, no steady-state.

Although it appears as Norströmsgrund's vibration response varies more than for other structures exposed to IIV, these response differences are also reported from structures located in different areas. In the Gulf of Finland, resonant vibrations were measured on the Hanko-1 channel marker on February 24, 2003 and March 6, 2003 (Fig. 11) (Määttänen, 2003; Määttänen, 2008). The first event showed steady-state FLI vibrations (Fig. 11a), whereas the second event showed less steady-state character (Fig. 11b). The first event was found to have a dominant frequency component near the first natural frequency (Fig. 11c), whereas the second event was found to have a dominant frequency component close to one of the higher modes (Fig. 11d).

Similarities between the February 24 event and a Norströmsgrund event (Fig. 12) can be seen comparing the frequency ranges 1-10 Hz for Hanko-1 (Fig. 11c) and 1-5 Hz for Norströmsgrund (Fig. 12b); the most striking difference is that the Hanko-1 steel structure has much higher contributions in the higher modes. The modal damping and the force influence at the ice action point to the modes are important for determining which modes are susceptible to FLI and thus influence its signature. The signature of resonant vibrations found for one structure is therefore not necessarily a valid signature for other structures and may largely be influenced of the sensor location. Consequently, there are measurements in field and laboratory of vibrations that fall outside the definition of FLI used in the standard. As a result, uncertainty in fatigue life predictions and confusion exists around the definition of FLI. More full-scale time series of ice-induced vibrations may lead to precise signatures of regimes of ice-induced vibrations, which in turn influence how to design structures and how to design laboratory experiments; such data may elucidate the most important and least understood process, namely, the occurrence of FLI.

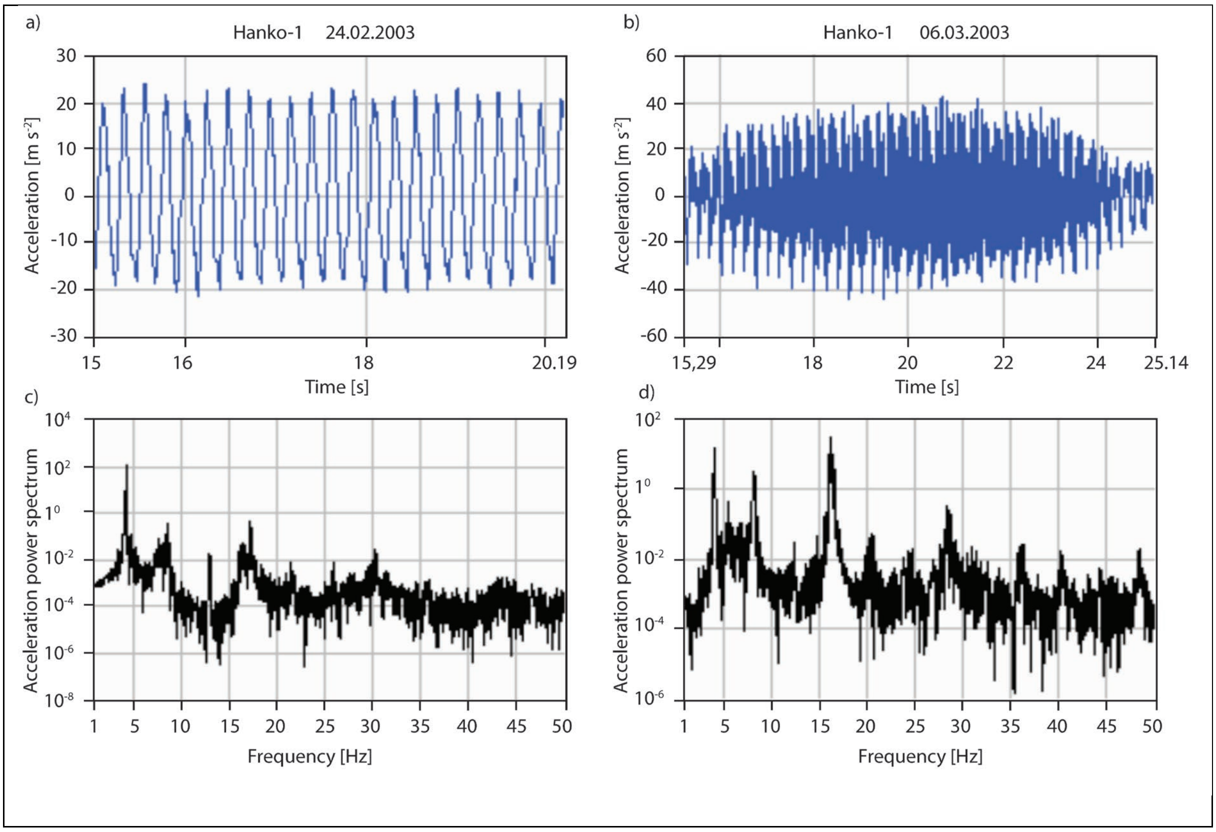

Fig. 11. Vibration events of the Hanko-1 Channel Marker: a) and b) time series of acceleration, c) and d) power spectrum of the acceleration (Courtesy of Määttänen (2003)).

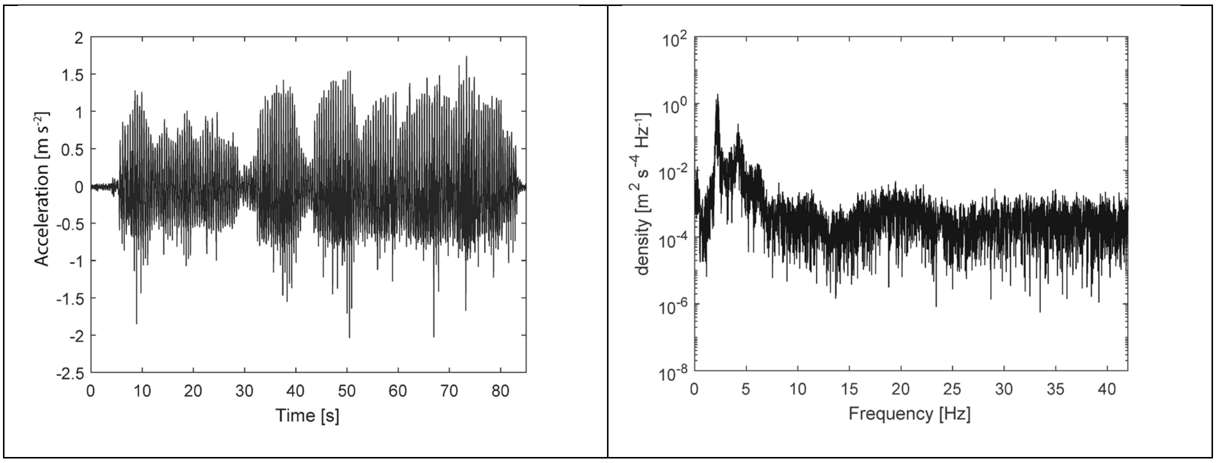

Fig. 12. Vibrations on Norströmsgrund lighthouse March 30, 2003: a) time series plot of acceleration and b) power spectral density of acceleration (from Nord et al. (2016)).

5.2 The occurrence aspect

The events of resonant vibrations occurred for days with very different FDDs; however, for each year, little increase in the FDD occurred after the last day of resonant vibrations (cf. Fig. 4). Besides the observations that the resonant vibrations on Norströmsgrund occurred when the ice concentration exceeded 0.85, the ice thickness exceeded 0.26 m and the ice velocity exceeded 0.023 m s^{-1}, the onset conditions remain unsolved. Several ice thicknesses and ice velocities that were present during resonant vibrations overlap with instances where other modes of ice-structure interaction were present. The wider the structure, the more susceptible it becomes to failure modes other than crushing (Daley et al., 1998; Sanderson, 1988; Timco, 1987), and with the great uncertainty in the ice thickness and ice velocity, predicting the failure mode becomes difficult.

The ice drift in the northern Gulf of Bothnia is mainly driven by winds, and local ice drift near Norströmsgrund is also influenced by the lead created by ice breakers and the edge to the landfast ice. The Farstugrund lighthouse, which is located approximately 29 km northeast of Norströmsgrund, has a slightly stiffer substructure and was equipped with the same data acquisition system for monitoring vibrations during the winter of 1988. Engelbrektson (1989) noted only a few events of resonant vibrations on the Farstugrund lighthouse during the full 1988 winter season (the days are marked with squares in Fig. 4) and explained this observation by more stationary ice conditions than those at Norströmsgrund.

Bjerkås et al. (2012) showed that, from February 14 to March 31 in 2003, a large lead opened in the northern Gulf of Bothnia. They estimated the open lead to be 15 km wide, although little is known about the time history of the lead opening. It was possible to track the ice thickness spatiotemporal variation using the ice thickness reanalysis available in the E.U. Copernicus Marine Service Information. March 25 and March 30 were the days in the STRICE project that had the most events of resonant vibrations. No significant changes were discovered around March 25, whereas from the evening on March 30 until the afternoon on March 31, the ice thickness (Fig. 13) and the ice concentration in the northern Gulf of Bothnia changed significantly. As most events of resonant vibrations occurred during the daytime and early afternoon, it is unclear whether the days in which drastic changes occur in the whole ice cover in northern Gulf of Bothnia are the days to expect resonant vibrations.

Temperature affects the ice mechanical properties through the porosity, and many of the events in 2001-2003 occurred during days in which the air temperatures exceeded 0°C. The mean and standard deviation of the air temperatures were -0.29°C and 2.58°C, respectively. Four events occurred at air temperatures less than -4°C, and four events had air temperatures greater than +4°C. Bjerkås et al. (2013a) estimated ice growth from FDD and studied measured ice temperature profiles collected at Norströmsgrund, and discussed their influence on the crushing behavior and occurrence of frequency lock-in vibrations. They showed that the temperature profiles changed from linear on February 28 in 2003 to irregular and c-shaped on March 9 and 10, respectively. March 9 and 10 were the first days during which resonant vibrations occurred that winter (Table 2). Their observations of the changed crushing behavior together with the decaying ice growth (Fig. 4a) and changed ice temperature profiles led to the hypothesis stating that frequency lock-in vibrations were more likely to occur late in winter because high ice temperatures would cause a more uniform contact at the ice-structure interface. However, Fig. 4a also shows considerable increase in FDD between end of February to mid-March in 1988, also a time period during which resonant vibrations occured. Despite this increase in FDD, it does not necessarily refute the hypothesis of Bjerkås et al. (2013a), as other factors may influence the ice temperature profile, and thus the mechanical properties.

Little is reported on floe size and confinement around structures susceptible to resonant vibrations. As more abundant and accurate met-ocean data can be retrieved for today's ice conditions in the Baltic Sea, new measurements of resonant vibrations and FLI may be better understood.

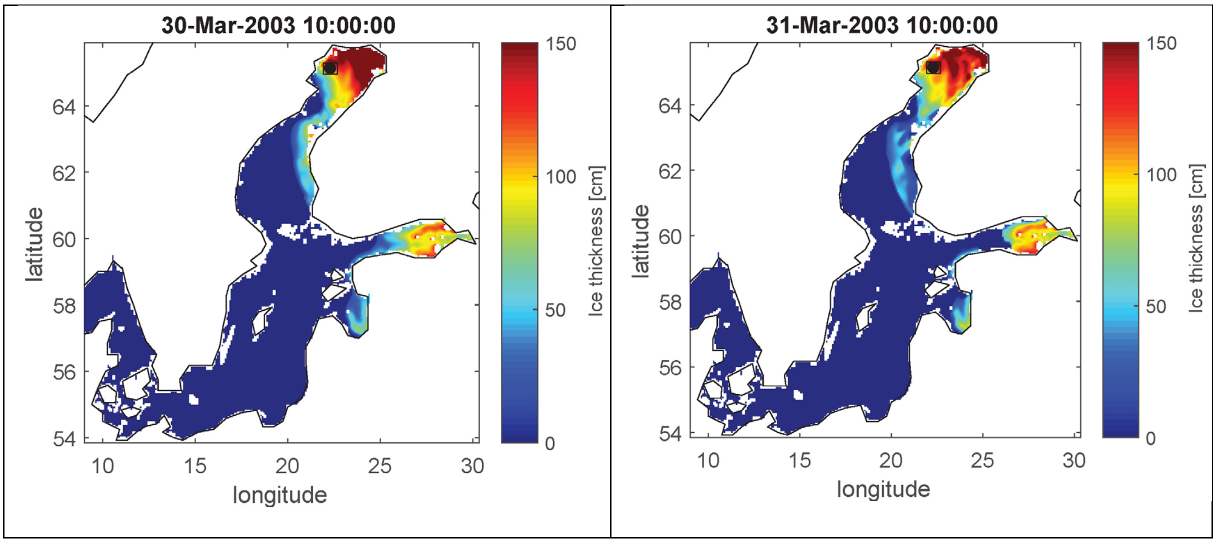

Fig. 13. HIROMB model estimate of the ice thickness on March 30-31, 2003.

6 Conclusions

Available data on the Norströmsgrund lighthouse in the northern Baltic were examined, and events with resonant vibrations were identified and discussed. For the STRICE data collected between 2001 and 2003, all time series of accelerations were used to identify events of resonant vibrations and to understand their inherent characteristics, i.e., their so-called signature. An attempt was further made to quantify the ice conditions for which resonant vibrations occur. The major findings can be summarized as follows:

- Sixty-one events of ice-induced vibrations measured on the Norströmsgrund lighthouse were classified as resonant vibrations between 2001 and 2003. The events were governed by response oscillations with a dominant frequency component between 2 and 2.7 Hz, with most between 2.2 and 2.4 Hz.
- Steady-state acceleration responses were seldom observed.
- The events encompassed level ice, rafted ice and ridges, in which ice thicknesses and ice velocities ranged from 0.26 to 1.9 m and from 0.023 to 0.075 m s^{-1}, respectively.

The longest event lasted for 100 seconds, and the average event lasted 22 seconds, which is significantly shorter than FLI reported on other structures.

- All events occurred on days in which the ice concentration was estimated as 0.85 or greater.

The results were compared with measurements of resonant vibrations from 1979-1988. In summary, most events occurred in the winter of 1988, followed by the winters of 2003 and 1980.

Furthermore, once resonant ice-induced vibrations violate the steady-state signature of FLI, they fall outside definitions of modes of ice-induced vibrations in the standards. Because the strongest resonant vibrations of Norströmsgrund violated this steady-state condition, we suggest that the steady-state or sinusoidal response is not a necessary and sufficient condition for FLI.

7 Acknowledgements

The authors wish to acknowledge the support of the Research Council of Norway through the Centre for Research-based Innovation, SAMCoT and the support of the SAMCoT partners. The full-scale measurements were funded by the European Commission DG RESEARCH under the Fifth Framework Program for Research and Development within the Energy, Environment and Sustainable Development (EESD) Program under the Key Action RTD activities of a generic nature (Contract No. EVG1-CT-2000-00024).

The authors wish to further acknowledge Lennart Fransson, Peter Jochmann and Mauri Määttänen for their efforts to provide information and insight to the measurements of ice-induced vibrations in the Baltic Sea.

Appendix A Acceleration time series of resonant vibrations at +37.1 m elevation.

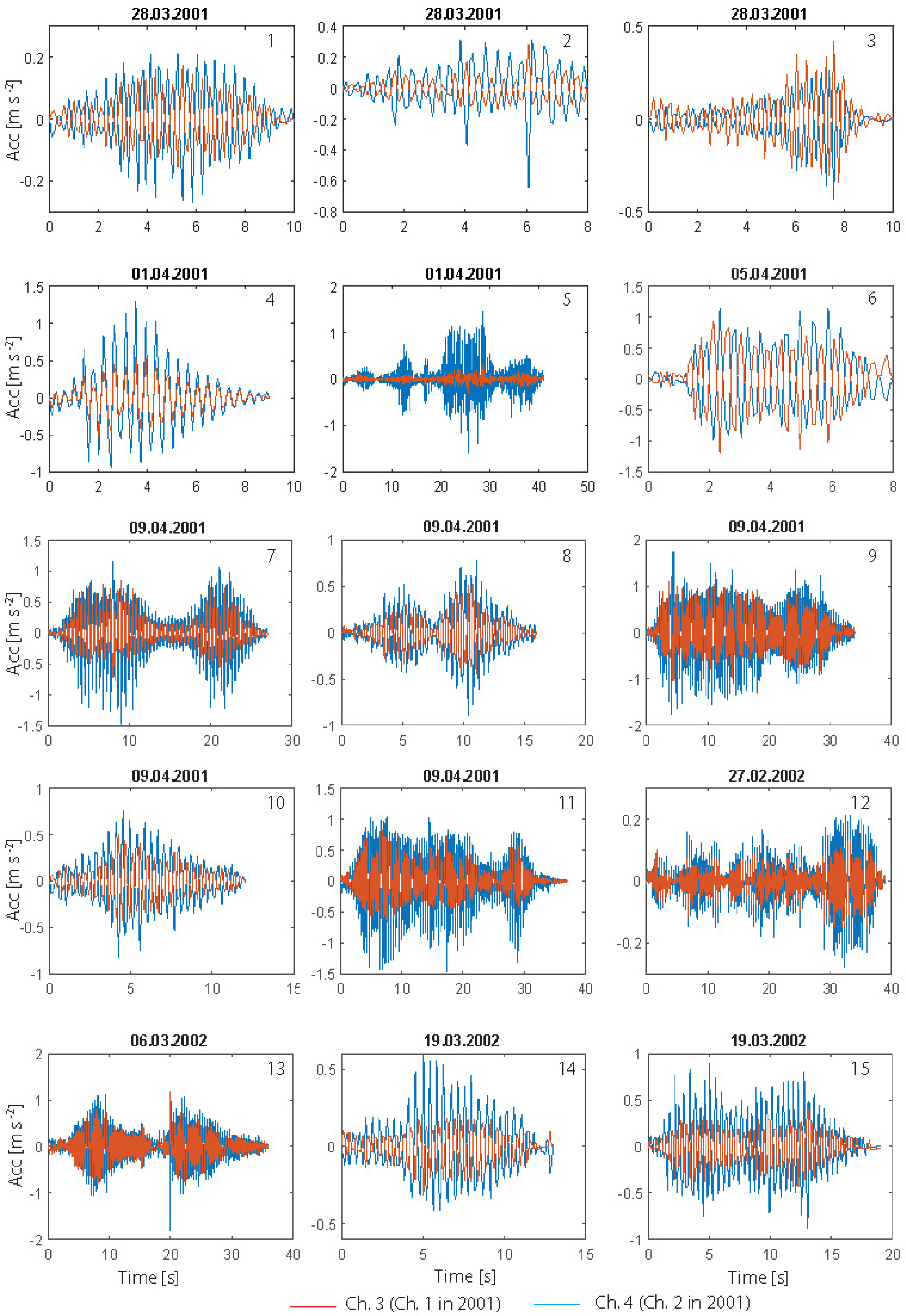

Fig. 14. Acceleration time series of resonant vibrations at +37.1 m elevation. Red and blue colors correspond to acceleration channels 3 and 4, respectively (in 2001 channels 1 and 2).

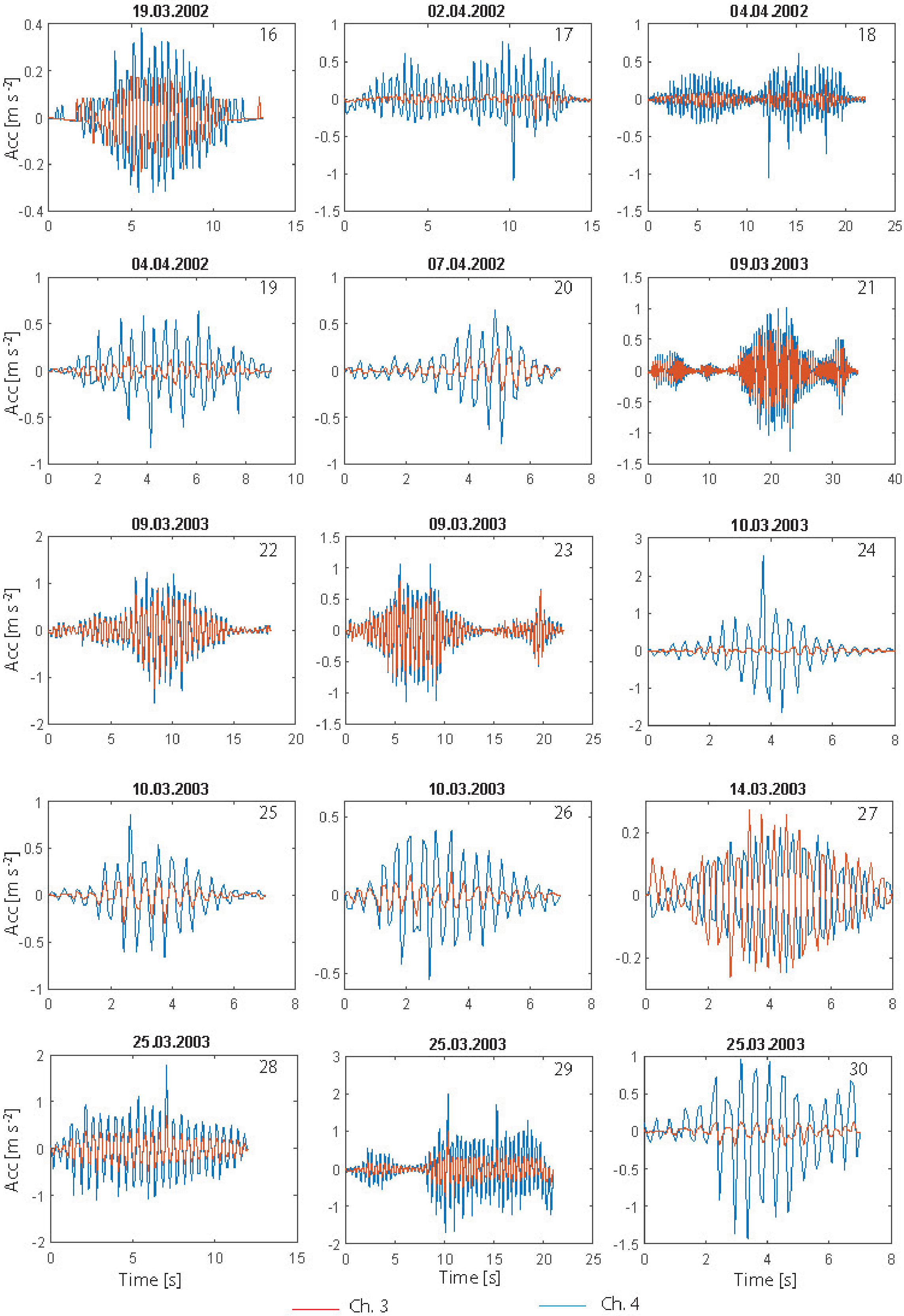

Fig. 15. Acceleration time series of resonant vibrations at +37.1 m elevation. Red and blue colors correspond to acceleration channels 3 and 4, respectively.

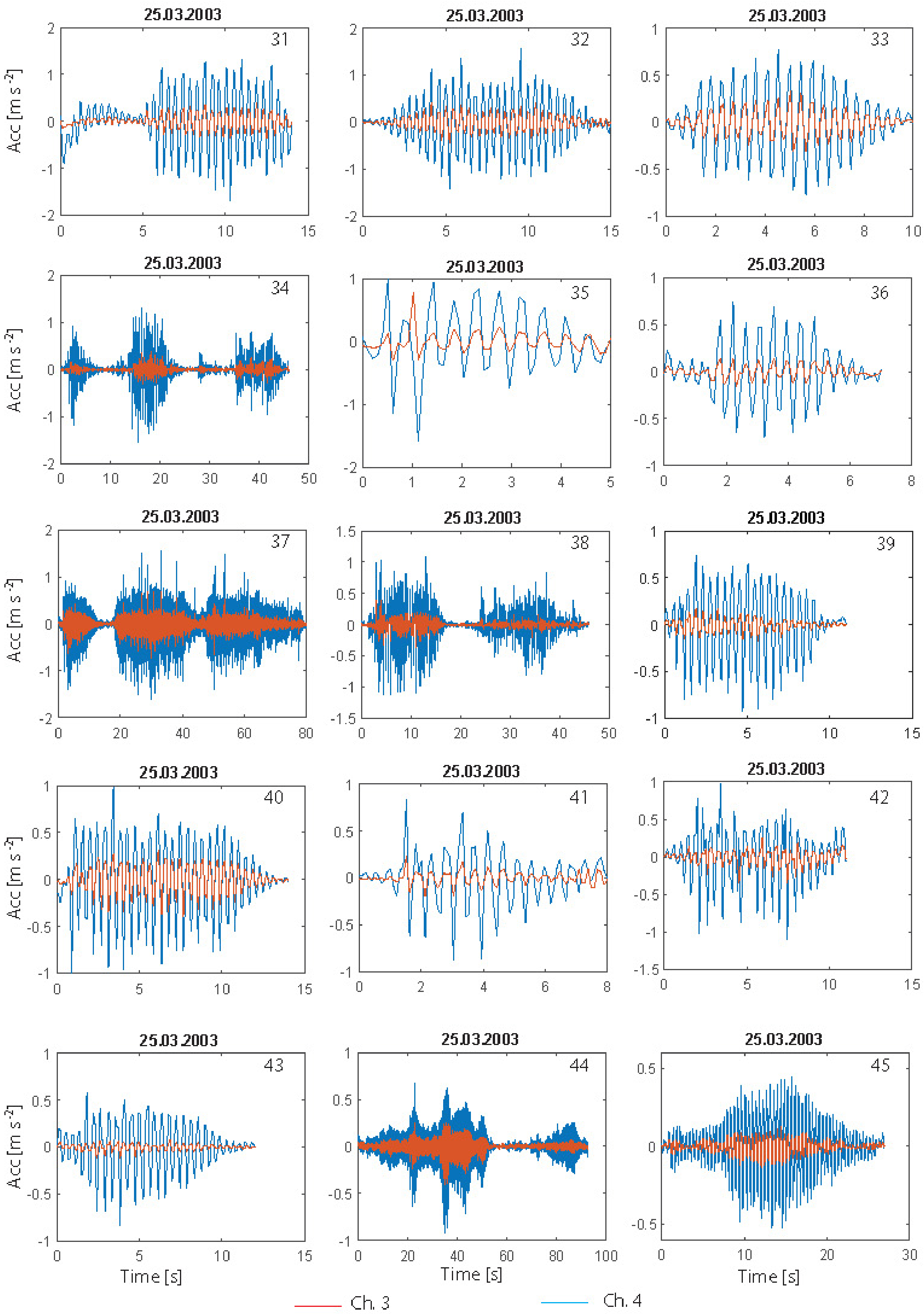

435

436 **Fig. 16.** Acceleration time series of resonant vibrations at +37.1 m elevation. Red and blue
437 colors correspond to acceleration channels 3 and 4, respectively.

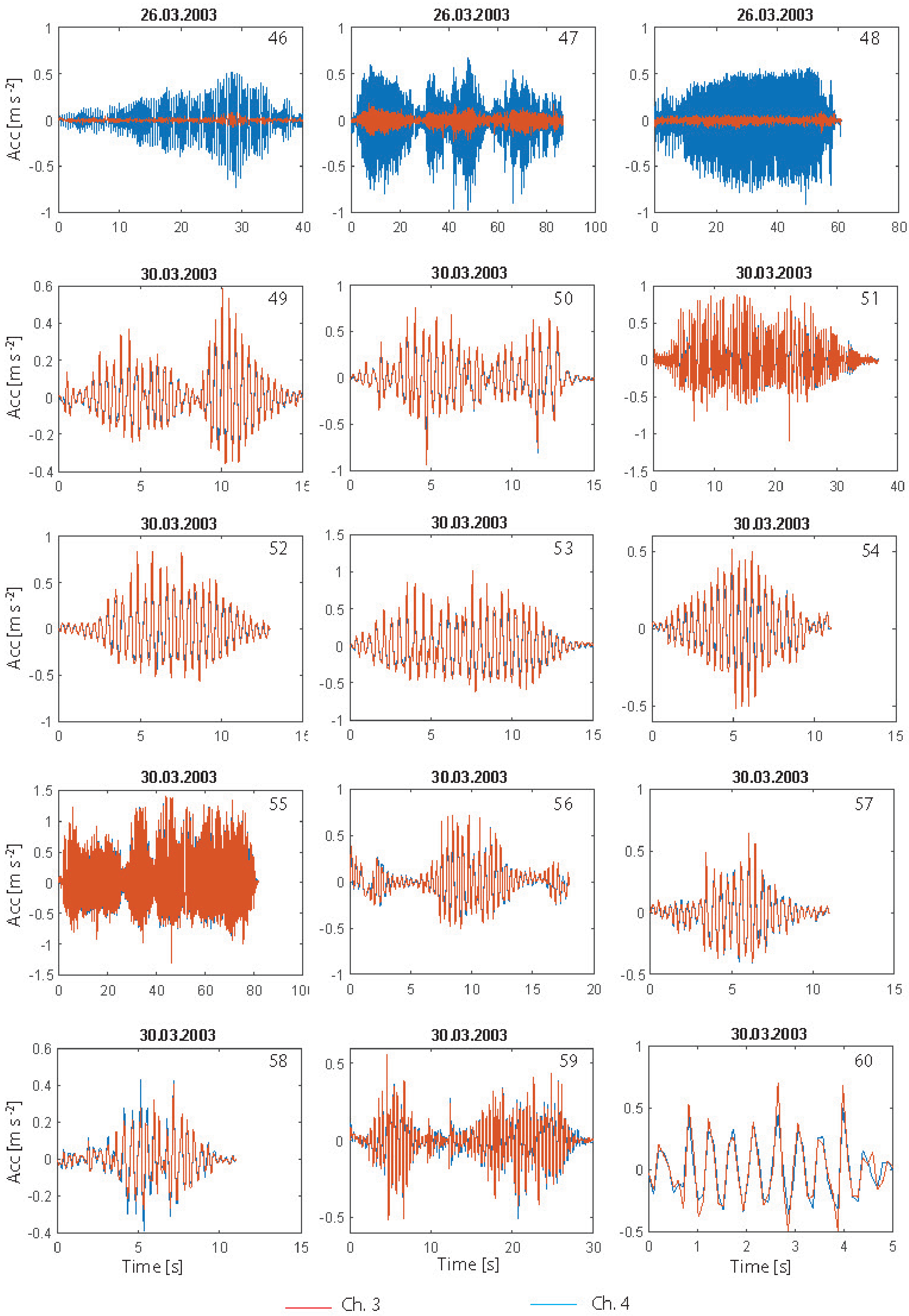

Fig. 17. Acceleration time series of resonant vibrations at +37.1 m elevation. Red and blue colors correspond to acceleration channels 3 and 4, respectively.

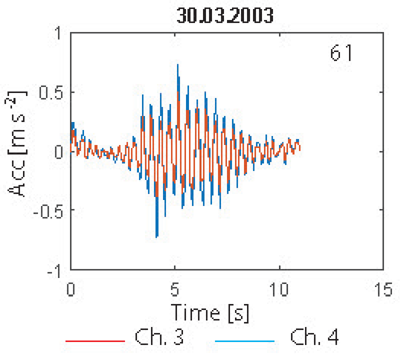

Fig. 18. Acceleration time series of resonant vibrations at +37.1 m elevation. Red and blue colors correspond to acceleration channels 3 and 4, respectively.

References

Axell, L., Golbeck, I., Jandt, S. and Izotova, J., 2017. Quality information document, Baltic Sea Production Centre BALTICSEA_REANALYSIS_PHYS_003_008, Copernicus marine environment monitoring service.

Bjerkås, M., 2006a. Ice action on offshore structures. PhD Thesis, NTNU, ISBN 82-471-7756-0, 173 pp.

Bjerkås, M., 2006b. Wavelet transforms and ice actions on structures. Cold Regions Science and Technology, 44(2): 159-169.

Bjerkås, M. and Bonnemaire, B., 2004. Ice ridge-structure interaction Part II: Loads from first-year ice ridges and their surronding ice sheets, 17th IAHR International Symposium on Ice, St. Petersburg, Russia, pp. 122-129.

Bjerkås, M., Lønøy, C. and Gürtner, A., 2012. Seasonal Variations in the Occurrence of Ice Induced Vibration of a Bottom Fixed Structure, Proceedings of the Twenty-second International Offshore and Polar Engineering Conference (ISOPE), Rhodes, Greece, pp. 1358-1364.

Bjerkås, M., Lønøy, C. and Gürtner, A., 2013a. Ice-Induced Vibrations and Effects of Ice Temperature. International Journal of Offshore and Polar Engineering, 23(1): 9-14.

Bjerkås, M., Meese, A. and Alsos, H.S., 2013b. Ice Induced Vibrations- Observations of a Full-Scale Lock-in Event, Proceedings of the Twenty-third International Offshore and Polar Engineering International Society of Offshore and Polar Engineers (ISOPE), Anchorage, Alaska, pp. 1272-1279.

Blenkarn, K.A., 1970. Measurment and analysis of ice forces on Cook Inlet structure, Offshore Technology Conference, Houston, TX, pp. 365-378.

Daley, C., Tuhkuri, J. and Riska, K., 1998. The role of discrete failures in local ice loads. Cold Regions Science and Technology, 27(3): 197-211.

E.U.Copernicus, 2017. BALTICSEA_REANALYSIS_PHYS_003_008. In: C.M.E.M. Service (Editor).

Engelbrektson, A., 1977. Dynamic ice loads on a lighthouse structure, Fourth international conference on Port and Ocean engineering under Arctic Conditions (POAC), St. John's, Newfoundland, Canada, pp. 654-663.

Engelbrektson, A., 1983. Observations of a resonance vibrating lighthouse structure in moving ice, The seventh international conferene on port and ocean engineering under arctic conditions, Espoo, Finland, pp. 855-864.

Engelbrektson, A., 1987a. Introductory study of ice-induced vibrations. Analysis of field observations from Norströmsgrund lighthouse during the period 1979-1985. Report No. 2, VBB,National Administration of Shipping and Navigation, University of Luleå.

Engelbrektson, A., 1987b. Methods for Structural Response Measurements and their Transformation to Ice Forces, Report No. 3, VBB, The National Swedish Administration of Shipping and Navigation, University of Luleå.

Engelbrektson, A., 1989. Ice force studies in the Bothnian Bay 1985-1988, Report No. 5, summary report, VBB, The National Swedish Administration of Shipping and Navigation, University of Luleå.

Engelbrektson, A. and Janson, J.E., 1985. Field Observations of Ice Action on Concrete Structures in the Baltic Sea. Concrete International, 7(8): 48-52.

Fransson, L. and Stenman, U., 2004. Mechanical properties of ice at Norströmsgrund, Tests 2003, Deliverable No. D-4.3.3., Luleå University of Technology, Sweden.

Haas, C., 2000. LOLEIF report: EM thickness measurements at the lighthouse Norströmsgrund. Part 1: system installation, modelling and calibration.

Haas, C. and Jochmann, P., 2003. Continuous EM and ULS thickness profiling in support of ice force measurements, Proceedings of the 17th International Conference on Port and Ocean Engineering under Arctic Conditions (POAC), Trondheim, Norway.

Haas, C., Jochmann, P., Gehrish, S., Kärnä, T., Kolari, K., Bjerkås, M., Bonnemaire, B. and Grösland, R., 2003. Full scale measurements at Lighthouse Norströmsgrund –winter 2003-Annex H2 EM ice thickness measurements.

Hendrikse, H., 2017. Ice-induced vibrations of vertically sided offshore structures, Delft University of Technology, 155 pp.

Hendrikse, H. and Metrikine, A., 2015. Interpretation and prediction of ice induced vibrations based on contact area variation. International Journal of Solids and Structures, 75–76: 336-348.

ISO, 2010. ISO/FDIS 19906, pp. 188.

Jefferies, M.G. and Wright, W.H., 1988. Dynamic response of "Molikpaq" to ice-structure interaction, Proc. 7th International conference on Offshore Mechanics and Arctic Engineering (OMAE 88), Houston, Texas, United States, pp. 201-220.

Jochmann, P. and Schwarz, J., 1999. Ice force measurements at lighthouse Norströmsgrund- winter 1999, LOLEIF Report No. 5, MAS3-CT-97-0098, Hamburgische shiffbau-versuchsantalt GmbH.

Kärnä, T., 1994. Steady-state vibrations of offshore structures. Hydrotechnical Construction, 28(8): 446-453.

Kärnä, T. and Jochmann, P., 2003. Field observations on failure modes, Port and Ocean Engineering under Arctic Conditions, Trondheim, Norway, pp. 839-849.

Kärnä, T. and Yan, Q., 2009. Analysis of the size effect in ice crushing- edition 2, VTT INTERNAL REPORT, RTE50-IR-6 , Ver. 1.3.

Leese, J.A., Novak, C.S. and Clark, B.B., 1971. An Automated Technique for Obtaining Cloud Motion from Geosynchronous Satellite Data Using Cross Correlation. Journal of Applied Meteorology, 10(1): 118-132.

Li, H., Bjerkås, M., Høyland, K.V. and Nord, T.S., 2016. Panel loads and weather conditions at Norströmsgrund lighthouse 2000-2003, 23rd IAHR International Symposium on Ice Ann Arbor, Michigan, USA, ISSN: 2414-6331, pp. 10.

Määttänen, M., 1975. Experiences of ice forces against a steel lighthouse mounted on the seabed, and proposed constructional refinements, Port and Ocean Engineering under Arctic conditions (POAC), Fairbanks, Alaska, pp. 857-867.

Määttänen, M., 2003. Hanko 1 reunamerkin värähtelymittaukset talvella 2003, Helsinki University of Technology, Laboratory of Mechanics and Materials.

Määttänen, M., 2008. Ice velocity limit to frequency lock-in vibrations, International symposium on Ice, IAHR, Vancouver, Canada, pp. 1265-1276.

Nord, T.S., Kvåle, K.A., Petersen, Ø.W., Bjerkås, M. and Lourens, E.-M., 2017. Operational modal analysis on a lighthouse structure subjected to ice actions. Procedia Engineering, 199: 1014-1019.

Nord, T.S., Øiseth, O. and Lourens, E.-M., 2016. Ice force identification on the Norströmsgrund lighthouse. Computers & Structures, 169(Supplement C): 24-39.

Nordlund, O.P., Tuomo, K. and Järvinen, E., 1988. Measurements of ice-induced vibrations of channel markers, IAHR Ice Symposium, Sapporo, Japan, pp. 537-548.

Peyton, H.R., 1967. Sea Ice Strength, University of Alaska.

Rajasekar, S. and Sanjuan, M.A.F., 2016. Harmonic and Nonlinear Resonances, Nonlinear Resonances. Springer International Publishing, Cham, pp. 1-38.

Samardzija, I., 2018. Two applications of a cross-correlation based ice drift tracking algorithm; Ship-based marine radar images and camera images from a fixed structure, 24rd IAHR International Symposium on Ice, . Far Eastern Federal University, Vladivostok, Russia.

Sanderson, T.J.O., 1988. Ice Mechanics: Risks to Offshore Structures. Graham & Trotman, London, UK; Boston.

Sodhi, D.S., 1988. Ice-induced vibration of structures, Proceedings of the 9th IAHR International Symposium on Ice, Sapporo, Japan, pp. 625-657.

Timco, G.W., 1987. Indentation and Penetration of Edge-Loaded Freshwater Ice Sheets in the Brittle Range. Journal of Offshore Mechanics and Arctic Engineering, 109(3): 287-294.

Yue, Q. and Bi, X., 2000. Ice-Induced Jacket Structure Vibrations in Bohai Sea. Journal of Cold Regions Engineering, 14(2): 81-92.

Yue, Q., Guo, F. and Kärnä, T., 2009. Dynamic ice forces of slender vertical structures due to ice crushing. Cold Regions Science and Technology, 56(2–3): 77-83.

Yue, Q., Xiangjun, B., Zhang, X. and Tuomo, K., 2002. Dynamic ice forces caused by crushing failure, Proceedings of the 16th International Symposium on Ice Dunedin, New Zealand, pp. 134-141.

List of figure captions

Fig. 1. Illustration of the accelerometer and force panel locations and picture of the Norströmsgrund lighthouse.

Fig. 2. Schematic of the data processing flow.

Fig. 3. Response during a low-amplitude resonant vibration event (# 44 in Table 2).

Fig. 4. Seasonal overview of resonant vibration events: a) freezing degree days and days with resonant vibrations from 1979-2003 according to Li et al. (2016); b) number of events per month for different years.

Fig. 5. Acceleration (a), ice-drift velocity (b) and ice thickness (c) on April 5, 2001.

Fig. 6. Ice velocity versus duration of the events (a) and acceleration at the upper level versus ice velocity (b).

Fig. 7. Ice drift direction versus a) ice velocity and b) event peak acceleration at the top level.

Fig. 8. Ice thickness and ice concentration obtained from the HIROMB model displayed together with ice thickness measurements during the resonant vibrations events.

Fig. 9. Event duration versus ice thickness (a) and event peak acceleration at the top level versus ice thickness (b).

Fig. 10. Singular value colormap of a) resonant vibration events and b) other interaction regimes.

Fig. 11. Vibration events of the Hanko-1 Channel Marker: a) and b) time series of acceleration, c) and d) power spectrum of the acceleration (Courtesy of Määttänen (2003)).

Fig. 12. Vibrations on Norströmsgrund lighthouse March 30, 2003: a) time series plot of acceleration and b) power spectral density of acceleration (from Nord et al. (2016)).

Fig. 13. HIROMB model estimate of the ice thickness on March 30-31, 2003.

Fig. 14. Acceleration time series of resonant vibrations at +37.1 m elevation. Red and blue colors correspond to acceleration channels 3 and 4, respectively (in 2001 channels 1 and 2).

Fig. 15. Acceleration time series of resonant vibrations at +37.1 m elevation. Red and blue colors correspond to acceleration channels 3 and 4, respectively.

Fig. 16. Acceleration time series of resonant vibrations at +37.1 m elevation. Red and blue colors correspond to acceleration channels 3 and 4, respectively.

Fig. 17. Acceleration time series of resonant vibrations at +37.1 m elevation. Red and blue colors correspond to acceleration channels 3 and 4, respectively.

Fig. 18. Acceleration time series of resonant vibrations at +37.1 m elevation. Red and blue colors correspond to acceleration channels 3 and 4, respectively.

List of Tables